

# Experimental Results of Compressive Sensing Based Imaging in Ultrasonic Non-Destructive Testing

Aras Azimipناه and Shahram ShahbazPanahi

Faculty of Engineering and Applied Science, Department of Electrical, Software, and Computer Engineering

University of Ontario Institute of Technology, Oshawa, ON, Canada

Email: {aras.azimipناه, shahram.shahbazpanahi}@uoit.ca

**Abstract**—In this paper, we use sparse signal recovery for non-destructive testing application, where the image of a test sample is extracted from ultrasonic array data. Using a frequency-domain model for the received signals, we propose two rearrangements of the data model to convert it to the format needed for sparse signal recovery. Each proposed approach is tested on the experimental data and the performance is compared with a MUSIC based imaging algorithm. The first rearrangement uses the measurement data obtained from individual transmitter elements in the array at a single frequency bin. We call this approach incoherent compressive sensing (IncCS). The second rearrangement is based on multiple measurement vectors (MMV) model. While the IncCS image has less background noise, the MMV results show better resolution in imaging the targets in the region of interest (ROI). The performance of the proposed approaches is better than MUSIC based algorithm. The MMV results also show that by using only half of the ultrasonic elements in the array, we can obtain an image which has comparable performance with the image obtained using the full array data.

## I. INTRODUCTION

In the last decade, compressive sensing (CS) theory has emerged in the field of digital signal processing [1]. The theory suggests that for the family of sparse or approximately sparse signals, a much more efficient course of sampling and recovery method can be developed.

Ultrasonic non-destructive testing (NDT) is one of the areas where the need of evaluating huge amount of materials and surfaces demands quicker ultrasonic signal acquisition. An ultrasonic test is usually carried out on a material which is supposed to be in its good shape unless there is a crack, corrosion, or cavity inside. This motivates us to look at the NDT imaging as a sparse signal recovery problem and employ sparsity of the underlying image which has been ignored by other array processing based methods. Having said that, we are interested in developing a model which reflects the sparsity of the medium under test and in the next step use a sparse signal recovery approach to reconstruct the sparse image representing the characteristics of this medium.

CS aims to find a stable algorithm to solve an under-determined system of linear equations, while the unknown vector is known to be sparse. Stable signal recovery means that CS finds a solution which is unique, or in a probabilistic point of view, is close enough to the optimal unique solution. CS achieves stable signal recovery by using measurements whose length is much smaller than the size of the sparse signal. These measurements are collected in a non-adaptive manner

i.e., the measurement process is independent of the sparse signal. Consider the following noisy measurement model:

$$\mathbf{y} = \mathbf{A}\mathbf{c} + \mathbf{v} \quad (1)$$

where  $\mathbf{A} \in \mathbb{R}^{m \times n}$ . In (1),  $\mathbf{c} \in \mathbb{R}^n$  is the sparse signal,  $\mathbf{y}$  is the measurement vector, and  $\mathbf{v}$  is the measurement noise. A proposed convex approach to recover the sparse vector  $\mathbf{c}$  is

$$\min_{\mathbf{c}'} \|\mathbf{c}'\|_1 \text{ subject to } \|\mathbf{A}\mathbf{c}' - \mathbf{y}\|_2 \leq \epsilon. \quad (2)$$

This optimization problem is called basis pursuit de-noising (BPDN) [2]. In (2),  $\epsilon$  is the estimation of the variance of the noise.

Recently, joint sparse model or MMV model has attracted considerable attention in the field of CS ([3] and [4]). The aim of MMV problem is to identify the unknown common support of multiple measurements. These multiple measurements are made from signals which share roughly the same locations for their non-zero elements. The MMV formulation in a noiseless environment is

$$\mathbf{Y} = \mathbf{A}\mathbf{C} \quad (3)$$

where  $\mathbf{Y} \in \mathbb{R}^{m \times N}$  and  $\mathbf{C} \in \mathbb{R}^{n \times N}$ . In this notation,  $\mathbf{C}$  is the row sparse matrix which has only a few non-zero rows, and  $N$  is the number of multiple measurements. To measure the number of non-zero rows of  $\mathbf{C}$ ,  $\mathcal{K}$  is defined as  $\mathcal{K} = \|\mathbf{C}\|_{0,q}$  where  $\|\mathbf{C}\|_{r,q}$  is defined as

$$\|\mathbf{C}\|_{r,q} \triangleq \left( \sum_i \|\mathbf{C}(i, :)^T\|_q^r \right)^{1/r}. \quad (4)$$

Here,  $\mathbf{C}(i, :)$  is the  $i$ th row of matrix  $\mathbf{C}$ . Because of the non-convexity of  $l_0$ -norm, a relaxed version of the  $\mathcal{K}$  is introduced based on  $l_1$ -norm as  $\mathcal{R}(\mathcal{K}) = \|\mathbf{C}\|_{1,q}$ . A proposed solution to the MMV problem in the noisy scenario is obtained by solving the following optimization problem ([5] and [6]).

$$\min \|\mathbf{C}\|_{1,2} \text{ subject to } \|\mathbf{A}\mathbf{C} - \mathbf{Y}\|_{2,2} \leq \sigma. \quad (5)$$

This formulation is called MMV-BPDN. Different studies have used different combinations of  $r$  and  $q$  values. Choosing  $r$  determines the speed of convergence and also the sparsity of the solution to the problem. A smaller value of  $r$  speeds up the convergence, however it increases the likelihood of the algorithm getting trapped in a local minima [5]. A combination of  $r = 1$  with  $q = 2$  is studied in [6] and [7].

## II. DATA MODEL

Assume an array of  $N$  transducer elements are used to obtain an image of a test sample. The elements can both transmit and receive signals. Each time one element transmits signal and the they all receive the backscattered signal. Indices  $p$  and  $n$  are used for the element in transmission mode and that in receiver mode, respectively. We cover the ROI with a fine grid of  $L_g$  points. The distances of the transmitter-grid point ( $d_{lp}$ ) and grid point-receiver ( $d_{ln}$ ) paths are calculated as

$$d_{lp} = \sqrt{(x_p - x_l)^2 + z_l^2}, \quad d_{ln} = \sqrt{(x_n - x_l)^2 + z_l^2} \quad (6)$$

where in the Cartesian coordinate system, the  $p$ th transmitter, the  $n$ th receiver, and the  $l$ th grid point are located at  $(x_p, 0)$ ,  $(x_n, 0)$  and  $(x_l, z_l)$ , respectively. The received signal contaminated by the receiver noise is modeled as [8]

$$y_{np}(\omega) = \sum_{l=1}^{L_g} \frac{o_l H^{np}(\omega)}{\sqrt{d_{ln} d_{lp}}} e^{-jk(\omega)(d_{ln}+d_{lp})} F_p(\omega) + v_{np}(\omega) \quad (7)$$

where  $y_{np}(\omega)$  is the received frequency-domain data at frequency bin  $\omega$ , when the  $p$ th transmitter is transmitting and the  $n$ th receiver is receiving. The phase shifts of both transmit and receive paths are captured in the exponential term  $e^{-jk(\omega)(d_{ln}+d_{lp})}$ , where  $k(\omega) = \frac{\omega}{c}$  and  $c$  are the wavenumber and the ultrasonic wave propagation speed, respectively. In a 2-dimensional ROI, the beam spread governs the inverse power law, which is the reason why we use a square root for the attenuation factor in (7). In this model,  $v_{np}(\omega)$  denotes the corresponding observation noise when Transmitter  $p$  is transmitting and Receiver  $n$  is receiving the backscattered signal.  $H^{np}(\omega)$  captures both electrical-to-acoustic transfer function of the  $p$ th transmitter and the acoustic-to-electrical transfer function of the  $n$ th receiver.  $F_p(\omega)$  is the signal transmitted by the  $p$ th transmitter at frequency bin  $\omega$ . Finally,  $o_l$  is the reflection coefficient of the  $l$ th point on the grid and it is non-zero if there is a point reflector at this point. We assume that the transfer functions for all the transmitter-receiver elements of the transducer are the same, meaning that  $H^{np}(\omega) = H(\omega)$ . We also assume  $F_p(\omega)H(\omega) = 1$ . Using these assumptions, we can rewrite (7) in the following form:

$$y_{np}(\omega) = \sum_{l=1}^{L_g} \frac{1}{\sqrt{d_{ln} d_{lp}}} o_l e^{-jk(\omega)(d_{ln}+d_{lp})} + v_{np}(\omega). \quad (8)$$

A frequency-dependent near-field steering vector corresponding to the  $l$ th point on the grid is defined as

$$\psi_l(\omega) \triangleq \left[ \frac{e^{-jk(\omega)d_{l1}}}{\sqrt{d_{l1}}} \quad \frac{e^{-jk(\omega)d_{l2}}}{\sqrt{d_{l2}}} \quad \dots \quad \frac{e^{-jk(\omega)d_{lN}}}{\sqrt{d_{lN}}} \right]^T. \quad (9)$$

The received data vector and the measurement noise vector, when the  $p$ th transmitter is transmitting, are defined as

$$\begin{aligned} \mathbf{y}_p(\omega) &\triangleq [y_{1p}(\omega) \ y_{2p}(\omega) \ \dots \ y_{Np}(\omega)]^T \\ \mathbf{v}_p(\omega) &\triangleq [v_{1p}(\omega) \ v_{2p}(\omega) \ \dots \ v_{Np}(\omega)]^T. \end{aligned} \quad (10)$$

We further define  $s_p^l(\omega)$  as

$$s_p^l(\omega) \triangleq o_l \frac{1}{\sqrt{d_{lp}}} e^{-jk(\omega)d_{lp}}. \quad (11)$$

Using (9)-(11), the vector form of (8) is written as

$$\mathbf{y}_p(\omega) = \sum_{l=1}^{L_g} \psi_l(\omega) s_p^l(\omega) + \mathbf{v}_p(\omega). \quad (12)$$

Using the following definitions:

$$\Psi(\omega) \triangleq [\psi_1(\omega) \ \psi_2(\omega) \ \dots \ \psi_{L_g}(\omega)] \quad (13)$$

$$\mathbf{s}_p(\omega) \triangleq [s_p^1(\omega) \ s_p^2(\omega) \ \dots \ s_p^{L_g}(\omega)]^T \quad (14)$$

we rewrite (12) in the matrix form, as

$$\mathbf{y}_p(\omega) = \Psi(\omega) \mathbf{s}_p(\omega) + \mathbf{v}_p(\omega). \quad (15)$$

The data model is similar to the general model introduced in (1) which is used in the CS literature. In this model,  $\mathbf{s}_p(\omega)$  is a sparse vector.

## III. COMPRESSIVE SENSING BASED IMAGING

The non-zero entries of the vector formulated in (14) correspond to the point reflectors in the ROI. The entries of this vector are non-zero, if  $o_l$  in (11) belongs to a point reflector in the ROI. In this section, two approaches are proposed to recover  $\mathbf{s}_p(\omega)$ , based on sparse signal recovery methods.

### A. Incoherent Compressive Sensing

It is obvious from the model presented in (15) that the sparse vector  $\mathbf{s}_p(\omega)$  is a function of both transmitter index and angular frequency. This model suggests an incoherent processing in which one can solve different optimization problems for different transmitter indices at a chosen frequency bin. At a single-frequency bin, we solve  $N$  individual  $l_1$ -norm minimization problems of the form:

$$\hat{\mathbf{s}}_p(\omega) = \min_{\mathbf{s}'_p(\omega)} \|\mathbf{s}'_p(\omega)\|_1 \text{ s.t. } \|\mathbf{y}_p(\omega) - \Psi(\omega) \mathbf{s}'_p(\omega)\|_2 \leq \varepsilon \quad (16)$$

for  $p = 1, 2, \dots, N$ . It is assumed that  $\varepsilon$  is the same for all the  $l_1$ -norm minimization problems. Solving each minimization problem yields a complex sparse vector whose major coefficients are representing the non-zero elements of  $\mathbf{s}_p(\omega)$ . In the next step, these results are combined to obtain the final image of the ROI. A logical way to do this is to normalize each result by its own maximum value and sum them up for different transmitter indices. The logic behind normalization is that the coefficients are dependent on the distances from the transmitter elements in the array, and they are different in value for the same scatterer, when the transmitter index changes. This process yields the final image as

$$\mathcal{I}_{\text{Inc-CS}}(\omega) = \sum_{p=1}^N \left| \frac{\hat{\mathbf{s}}_p(\omega)}{\max(\hat{\mathbf{s}}_p(\omega))} \right| \quad (17)$$

where  $\mathcal{I}_{\text{Inc-CS}}(\omega)$  is the recovered sparse image, and  $\max(\hat{\mathbf{s}}_p(\omega))$  is with a small abuse of notation, the maximum of the entries of vector  $\hat{\mathbf{s}}_p(\omega)$ .

### B. Multiple Measurement Vectors

In (15), we can see that for different transmitter indices a common  $\Psi(\omega)$  is needed as the measurement matrix. This suggests that we can arrange all the  $N$  measurement vectors at the frequency bin  $\omega$ , in a matrix  $\mathbf{Y}(\omega)$  of size  $N \times N$  as

$$\mathbf{Y}(\omega) = [\mathbf{y}_1(\omega) \ \mathbf{y}_2(\omega) \ \dots \ \mathbf{y}_N(\omega)] \quad (18)$$

and consider the problem as an MMV problem. Using the multiple images, the row-sparse matrix  $\mathbf{S}(\omega) \in \mathbb{R}^{L_g \times N}$  is built as

$$\mathbf{S}(\omega) = [\mathbf{s}_1(\omega) \ \mathbf{s}_2(\omega) \ \dots \ \mathbf{s}_N(\omega)]. \quad (19)$$

The MMV model at each frequency bin is

$$\mathbf{Y}(\omega) = \Psi(\omega)\mathbf{S}(\omega) + \mathbf{V}(\omega) \quad (20)$$

where  $\mathbf{V}(\omega) = [\mathbf{v}_1(\omega) \ \mathbf{v}_2(\omega) \ \dots \ \mathbf{v}_N(\omega)]$  is the noise matrix. We assume that  $\mathbf{v}_p(\omega)$  has the same variance. In the model we used, the row sparse property holds true because the images in (19) are identical except for some slightly differences in the amplitude of the entries of  $\mathbf{s}_p(\omega)$ , for different  $p$  indices. In the recovery step, we use a mixed norm convex optimization approach of the form of (5), i.e.,

$$\hat{\mathbf{S}}(\omega) = \min \|\mathbf{S}'(\omega)\|_{1,2} \quad \text{s.t.} \quad \|\Psi(\omega)\mathbf{S}'(\omega) - \mathbf{Y}(\omega)\|_{2,2} \leq \sigma \quad (21)$$

where  $\sigma$  is a user parameter which represents the estimation of the noise variance level. The MMV image is obtained by averaging all columns of  $\hat{\mathbf{S}}(\omega)$  into a vector.

### IV. ASSESSMENT

In this study, we use a 5MHz, 64-element linear phased array transducer to image several cylindrical side drilled holes in an aluminium block (Fig. 1). The array has an active aperture of 38.4mm, element pitch of 0.6mm and sampling rate of 100MHz. A grid of size  $L_g = 16275$  is considered for the experiment. The aperture of ultrasound array transducer is covering 3 holes. To solve the  $l_1$ -norm minimization problems

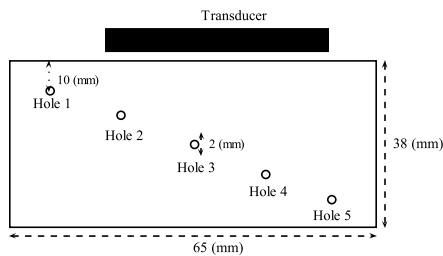


Fig. 1: The schematic of the experiment setup

we use CVX [9] and the MMV problems are solved using SPGL1 [10]. After doing multiple tests to determine the best parameter values, the MUSIC image is obtained using a signal subspace dimension of 40. We plot all the algorithms' images in the linear scale and to make a fair comparison possible, we normalize the result of each individual algorithm to its maximum value. This normalization will give us the images which are scaled from 0 to 1 in the gray scale. In the gray images, the closer the color to white, the higher the intensity of the point is, which indicates the location of the holes.

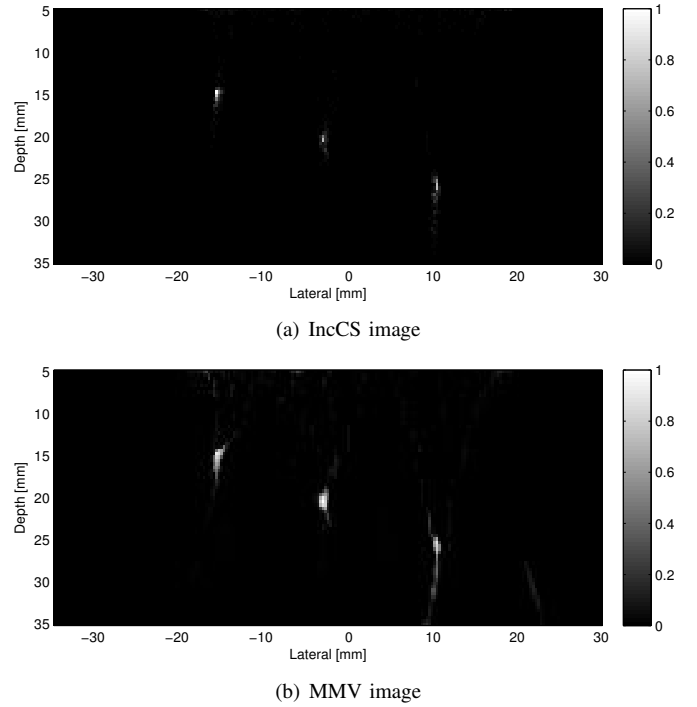


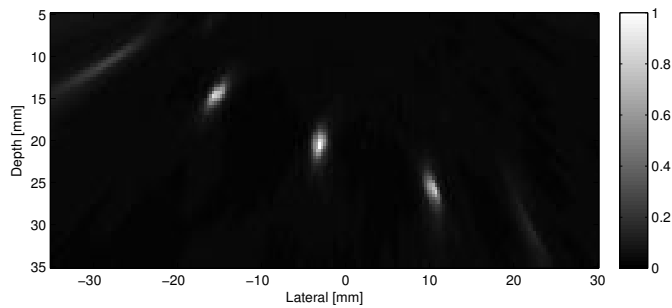
Fig. 2: Comparing IncCS and MMV images at a single frequency bin

### A. Results

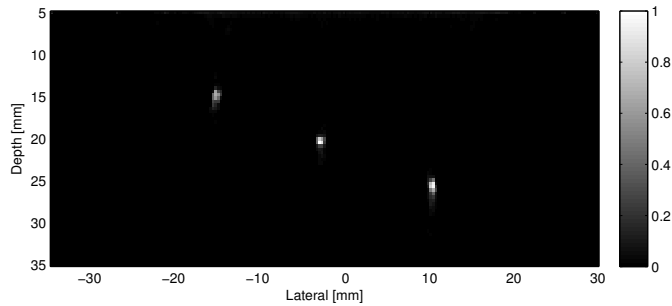
Fig. 2 shows the results of IncCS and MMV approaches, when a single frequency bin is used. Fig. 2(a) shows that IncCS approach is capable of imaging the three holes under the transducer array. This approach has failed to image Holes 1 and 5 in the corners. The MMV result, in Fig. 2(b), shows a higher resolution than the IncCS image. The MMV method is also capable of imaging wider area under the array by capturing Hole 5 in the image. However, we can see that the background noise in the incoherent processing image is less, compared to the MMV image. The MMV image provides a better estimation of the true diameter of the holes.

In the next step of our assessment, we have obtained the IncCS, MMV, and MUSIC images averaged over 6 frequency bins equally distanced between 5.1 MHz and 7.6 MHz (Fig. 3). Comparing the first three images in Fig. 3, we can see that the proposed CS based approaches show smaller sidelobe levels in the lateral and range directions compared to the MUSIC algorithm. The better resolution in the MMV image and its ability to capture Hole 5 are the advantages of using MMV over the incoherent compressive sensing. The MMV also provides a better estimation of the diameter of the holes, especially for Holes 2 and 3. A valuable observation in Fig. 3(c) is that averaging over different frequency bins has resulted in capturing Holes 1 and 5 in the ROI.

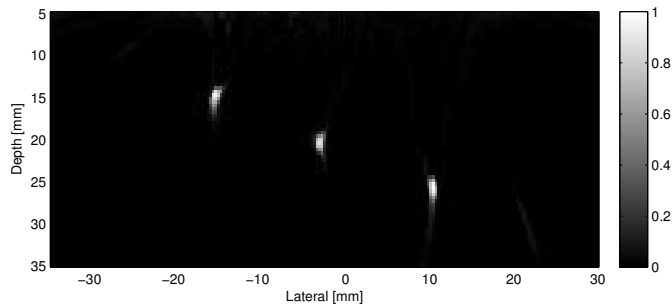
Finally, we test a situation where we now assume that our array has only the 32 odd indexed elements. We do this by removing the data from all the even indexed elements in the array, which results in a data matrix of the size of  $32 \times 32$ . The MMV approach is applied to this data and the averaged



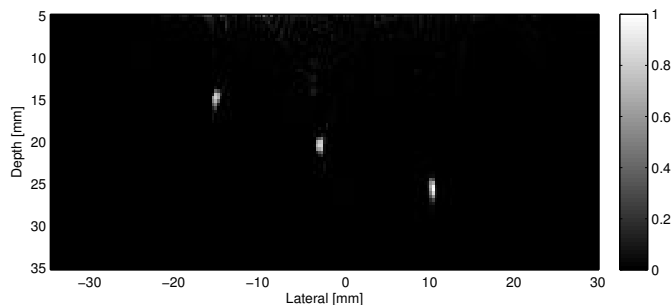
(a) MUSIC at signal subspace 40



(b) IncCS



(c) MMV full array



(d) MMV half array

Fig. 3: Comparing the MUSIC, MMV and IncCS images averaged over 6 frequency bins

image over 6 frequency bins is shown in Fig. 3(d). This figure shows that even using half array data we can achieve a very good performance in imaging the area under the transducer. The sidelobe level of the image in Fig. 3(d) is better compared to the MUSIC image.

The MMV test using full array data, shows a better estimation of the amplitude of Holes 2, 3 and 4 by providing

TABLE I: Maximum amplitude comparison for different algorithms

Holes $\Rightarrow$	1	2	3	4	5
Algorithm $\Downarrow$					
MUSIC	0.2872	0.8739	1	0.8369	0.1411
IncCS	0	0.6647	1	0.9345	0
MMV full array	0.0938	0.9225	0.8717	1	0.1241
MMV half Array	0	0.8020	0.8455	1	0

a closer values for the maximum amplitudes. This becomes obvious if we compare the amplitude values for the holes, as provided in Table I. In Table I, the maximum amplitudes of the normalized images of different algorithms are compared. In this table, the higher the value is the better the hole is distinguishable from the background. Also, closer values for the amplitude of the holes in each algorithm means that the algorithm better estimates the holes in different depths. The discussion about the sidelobe of different images in Fig. 3, and the values in Table I show that the CS based approaches can be considered as a promising practical approach in the NDT ultrasound imaging. The array location is such that holes 3 and 4 are in the center, this is why the intensity of the image at these holes is higher than the other holes.

## V. CONCLUSION

In this paper, using experimental results, we showed that the compressive sensing approach is a powerful tool which can be used in NDT ultrasound imaging. We also showed that coherent processing of the array data through multiple measurement vectors (MMV) will outperform the incoherent processing. And lastly, using MMV method we showed that only using half of the array elements, we achieve better performance than incoherent compressive sensing and the MUSIC algorithm in imaging the area below the transducer.

## REFERENCES

- [1] E. J. Candes, J. Romberg, and T. Tao, "Robust uncertainty principles: Exact signal reconstruction from highly incomplete frequency information," *IEEE Trans. Inf. Theory*, vol. 52, pp. 489–509, Feb. 2006.
- [2] S. S. Chen, D. L. Donoho, and M. A. Saunders, "Atomic decomposition by basis pursuit," *SIAM Rev*, vol. 43, pp. 129–159, Jan. 2001.
- [3] J. Chen and X. Huo, "Theoretical results on sparse representations of multiple-measurement vectors," *IEEE Trans. Signal Process.*, vol. 54, pp. 4634–4643, Dec. 2006.
- [4] E. Van Den Berg and M. P. Friedlander, "Theoretical and empirical results for recovery from multiple measurements," *IEEE Trans. Inf. Theory*, vol. 56, pp. 2516–4643, May 2010.
- [5] S. F. Cotter, B. D. Rao, K. Engang, and K. Kreutz-Delgado, "Sparse solutions to linear inverse problems with multiple measurement vectors," *IEEE Trans. Signal Process.*, vol. 53, pp. 2477–2488, Jul. 2005.
- [6] E. Van Den Berg and M. P. Friedlander, "Joint-sparse recovery from multiple measurements," *University of British Columbia, Technical Report*, pp. 1–19, Apr. 2009.
- [7] Y. C. Eldar and M. Mishali, "Robust recovery of signals from a structured union of subspaces," *IEEE Trans. Inf. Theory*, vol. 55, pp. 5302–5316, Nov. 2009.
- [8] F. Foroozan and S. Shahbazpanahi, "Music-based array imaging in multi-modal ultrasonic non-destructive testing," in *Proc. IEEE 7th SAM workshop*, 2012, pp. 529–532.
- [9] M. Grant and S. Boyd, "CVX: Matlab software for disciplined convex programming, version 2.0 beta," <http://cvxr.com/cvx>, Sep. 2012.
- [10] E. Van Den Berg and M. P. Friedlander, "SPGL1: A solver for large-scale sparse reconstruction," June 2007, <http://www.cs.ubc.ca/labs/scl/spgl1>.